Environmental Science & Technology

pubs.acs.org/est

Article

Reactive Nitrogen Hotspots Related to Microscale Heterogeneity in Biological Soil Crusts

Alexandra Maria Kratz,*[,⊥] Stefanie Maier,[⊥] Jens Weber,[⊥] Minsu Kim, Giacomo Mele, Laura Gargiulo, Anna Lena Leifke, Maria Prass, Raeid M. M. Abed, Yafang Cheng, Hang Su, Ulrich Pöschl, and Bettina Weber*

Cite This: *Environ. Sci. Technol.* 2022, 56, 11865−11877

Read Online

ACCESS | Metrics & More | Article Recommendations | Supporting Information

ABSTRACT: Biocrusts covering drylands account for major fractions of terrestrial biological nitrogen fixation and release large amounts of gaseous reactive nitrogen (N_r) as nitrous acid (HONO) and nitric oxide (NO). Recent investigations suggested that aerobic and anaerobic microbial nitrogen transformations occur simultaneously upon desiccation of biocrusts, but the spatio-temporal distribution of seemingly contradictory processes remained unclear. Here, we explore small-scale gradients in chemical concentrations related to structural characteristics and organism distribution. X-ray microtomography and fluorescence microscopy revealed mixed pore size structures, where photoautotrophs and cyanobacterial polysaccharides clustered irregularly in the uppermost millimeter. Microsensor measurements showed strong gradients of pH, oxygen, and nitrite, nitrate, and ammonium ion concentrations at micrometer scales in both vertical and lateral directions. Initial oxygen saturation was mostly low (~30%) at full water holding capacity, suggesting widely anoxic conditions, and increased rapidly upon desiccation. Nitrite concentrations (~6 to 800 μM) and pH values (~6.5 to 9.5) were highest around 70% WHC. During further desiccation they decreased, while emissions of HONO and NO increased, reaching maximum values around 20% WHC. Our results illustrate simultaneous, spatially separated aerobic and anaerobic nitrogen transformations, which are critical for N_r emissions, but might be impacted by future global change and land management.

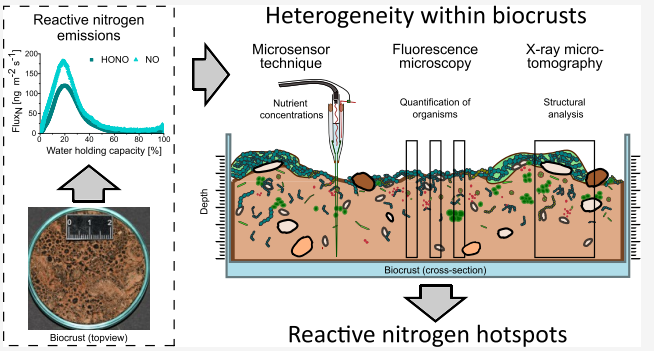

KEYWORDS: *biological soil crusts, reactive nitrogen, nitrous acid (HONO), nitric oxide (NO), microsensors, X-ray microtomography, fluorescence microscopy*

INTRODUCTION

Biological soil crusts (biocrusts) are assemblages of lichens, bryophytes, and microbes that colonize the uppermost layer of soil in dryland ecosystems and cover ~12% of the global terrestrial surface.[1−5] About 40% of the global terrestrial biological N fixation have been attributed to biocrusts,[6] sustaining soil fertility in nutrient-deprived dryland ecosystems.[7−9] Some of the fixed nitrogen can be re-emitted to the atmosphere in the form of nitrous oxide (N_2O),[10,11] ammonia (NH_3),[12,13] nitric oxide (NO), and nitrous acid (HONO).[14−23] The estimated global emissions of reactive nitrogen (N_r, HONO, and NO) amount to ~1.7 Tg a^{-1}, corresponding to ~20% of N_r from soils under natural vegetation cover.[20,24]

Nitrogen oxides (NO_x = NO + NO_2) and HONO are key species in the global N cycling and contribute to the production of tropospheric ozone (O_3, short-lived climate pollutant) and hydroxyl radicals ($OH^•$), which regulate the oxidizing power and self-cleaning capacity of the atmosphere.[25−31] N gas emissions from biocrusts, which host a special type of soil microbiome,[32] and soil may be mainly promoted by the biotic processes N-fixation, nitrification, and denitrification.[7,20,21,23,32−34] Under aerobic and anaerobic conditions in biocrusts and soil, nitrite (NO_2^-) can be formed during nitrification and denitrification, respectively, and can be released as HONO to the atmosphere.[7,20,21,23,32] Biological sources of NO include NH_3-oxidizing bacteria (AOB), which mediate the first phase of nitrification and carry out nitrifier denitrification under oxygen-limited conditions.[33,34]

NO and HONO emissions are known to be strongly related to the water content.[35] In most studies, emissions from drying soil and biocrusts were lowest at high water holding capacity

Received: March 30, 2022
Revised: July 12, 2022
Accepted: July 12, 2022
Published: August 5, 2022

(100% WHC) and reached maximum values around 20−30% WHC.[18,20,21,23] In another study, emissions of NO and HONO were shown to also occur at high water contents.[36] In former studies, HONO and NO emissions were analyzed by means of continuous flux measurements from bulk soil,[23] soil bacteria,[21] and biocrusts.[18,20,37] For biocrusts, a high variability in the total flux values was observed.[18,20,32] A drawback of flux measurements is, however, that they only give the integrated balance of gas exchange at the sample scale (∼cm), whereas they do not allow to draw conclusions at the scale relevant to microorganisms, substrate concentrations at microsites and processes occurring at pore scales. In former studies it has been observed that for example N_2O emissions occur in hotspots during hot moments, but to our knowledge this has not been described for N_r emissions, and the underlying small-scale processes have not been analyzed in detail.[38−40]

One method that allows such small-scale analyses is the application of microsensor techniques. The method of liquid ion-exchange (LIX) based microsensors has been developed to detect and analyze the concentrations of different ions, such as ammonium (NH_4^+), NO_2^-, nitrate (NO_3^-), and H^+ (pH). They have been used to conduct in-depth analyses of dynamic processes in artificial biofilms (in a porous substrate photobioreactor), as well as in wastewater biofilms and flocs to investigate the sulfate reduction and denitrification.[41,42] Johnson et al.[43] utilized LIX microsensors to directly measure the denitrification and nitrogen export in biocrusts to gain information on the fate of the fixed N.

In earlier studies, we observed that various, partly contradictory processes, such as N fixation, nitrification, denitrification, ammonification, and anaerobic ammonium oxidation (anammox), occur at the same time within a single piece of biocrust (see Figure 4c in Maier et al.[32]). Thus, the objective of this study was to understand how spatial heterogeneity within biocrusts and patterns in the local distribution of soil microbiota affect soil processes and hence gas fluxes at larger scales. The specific objectives were to (i) investigate the pore structure, utilizing X-ray microtomography (micro-CT) at different hydration stages, (ii) study the distribution of microbes in the microenvironments by means of fluorescence microscopy, and (iii) analyze the small-scale variation of physicochemical parameters (i.e., pH, O_2, and NH_4^+, NO_3^-, and NO_2^-) using microsensors under varying water contents. We aimed to address the influence of localized conditions of soil water, pH, NO_2^-, NO_3^-, and NH_4^+ on N_r emissions, especially HONO and NO, within a heterogeneous soil environment.

MATERIAL AND METHODS

Study Area. Samples for the analyses were collected next to the former BIOTA observatory of Soebatsfontein (30.1865°S, 17.5433°E, 392 m a.s.l), located within the Succulent Karoo biome, 60 km south of Springbok.[44−46] The Succulent Karoo is a semiarid dryland region, and its biome covers an area of about 103,000 km^2. This region is considered to be a diversity hotspot of global significance, which is mainly due to a high diversity of succulent plants, with many species being of major conservation importance.[47,48] At the observatory of Soebatsfontein, the temperature ranges from 3.5 °C (July) to 42.5 °C (February) with a mean air temperature of 19.4 °C.[37,45,46] The annual precipitation amounts to ∼131 (97−175) mm and most of the precipitation occurs between July and August with ∼45 precipitation events per year.[37,45,46,49]

Sampling. Cyanobacteria-dominated biocrusts with cyanolichens were collected in March, at the end of the dry season, in small Petri dishes (55 mm diameter and 10 mm height). For sampling, the bottom of the Petri dish was placed upside down on the biocrust surface, pressed into the substrate, and lifted with the help of a trowel pushed below. The samples were turned in an upright position and, in order to minimize metabolic activity, they were air-dried and subsequently transported to the Max Planck Institute for Chemistry (MPIC) in Mainz, Germany, for further analyses. For further details on the identification of species, refer to the Supporting Information, Methods.

X-Ray Microtomography. Structural analyses (pore size distribution and vertical porosity profiles) were performed with an X-ray microtomograph (micro-CT, Bruker 1272 system) using a scanning protocol with the parameters presented in Table S1A. Image reconstruction was conducted with NRecon software v. 1.7.1 applying the cone-beam algorithm of Feldkamp with the parameters indicated in Table S1B.

The crust sample chosen for the analysis was weighed (initial state), then saturated with distilled water and weighed again (Table S2). The crust structure was analyzed at the two states of ∼50 and 0% water holding capacity (WHC). For further details on the methodology, see the Supplementary Methods.

Fluorescence Microscopy. Fluorescence microscopy was used to localize and visualize photoautotrophic organisms (algae, cyanobacteria, cyanolichens) and complex polysaccharides [e.g., chitin, cellulose, and EPS (extracellular polymeric substances of cyanobacteria)], the latter indicating fungi and cyanobacterial sheaths in cross-sections of the cyanobacteria-dominated biocrusts. To assess the spatial distribution of photoautotrophic organisms, the autofluorescence of chlorophyll$_a$ was used. Complex polysaccharides were visualized using ready to use Calcofluor-White (CFW) stain. During fluorescence microscopy, two distinctive fractions of the biocrust samples were defined as photoautotrophic and heterotrophic layers (PL and HL, respectively) where the PL contains cyanobacteria, lichens, and bryophytes and the HL is devoid of photoautotrophs, but comprises fungi, bacteria, archaea, as well as microfauna (protozoa, nematodes and microarthropods). For further details regarding microscopy, see the Supplementary Methods.

Microsensor Measurements. Vertical concentration/saturation gradients were investigated during desiccation of biocrusts at 25 °C and in the dark, to be congruent with the conditions during dynamic chamber measurements. LIX sensors with a tip diameter of 20−30 μm were used for the determination of pH, NO_3^-, NO_2^-, and NH_4^+ concentrations and were produced as explained by de Beer et al.,[50−52] with slight adaptions for measurements in biocrust samples. In order to confer more stability, the sensor tips were thickened and cut with a diamond knife at the requested diameter of about 20−30 μm (inner diameter) under the microscope. pH measurements were obtained with LIX sensors and pH microelectrodes (pH-100, Unisense A/S, Aarhus, Denmark) with a tip diameter of 100 μm. O_2 saturation was analyzed using oxygen microsensors (OX-100, Unisense A/S, Aarhus, Denmark) with a tip diameter of 100 μm.

For the measurements, biocrust samples were saturated with sterile, artificial rainwater[53,54] and drained by gravity to achieve full WHC. The measurements were conducted during one desiccation cycle (wetting and subsequent drying). At least 15 vertical profiles were measured in the dark at hourly intervals

https://doi.org/10.1021/acs.est.2c02207
Environ. Sci. Technol. 2022, 56, 11865−11877

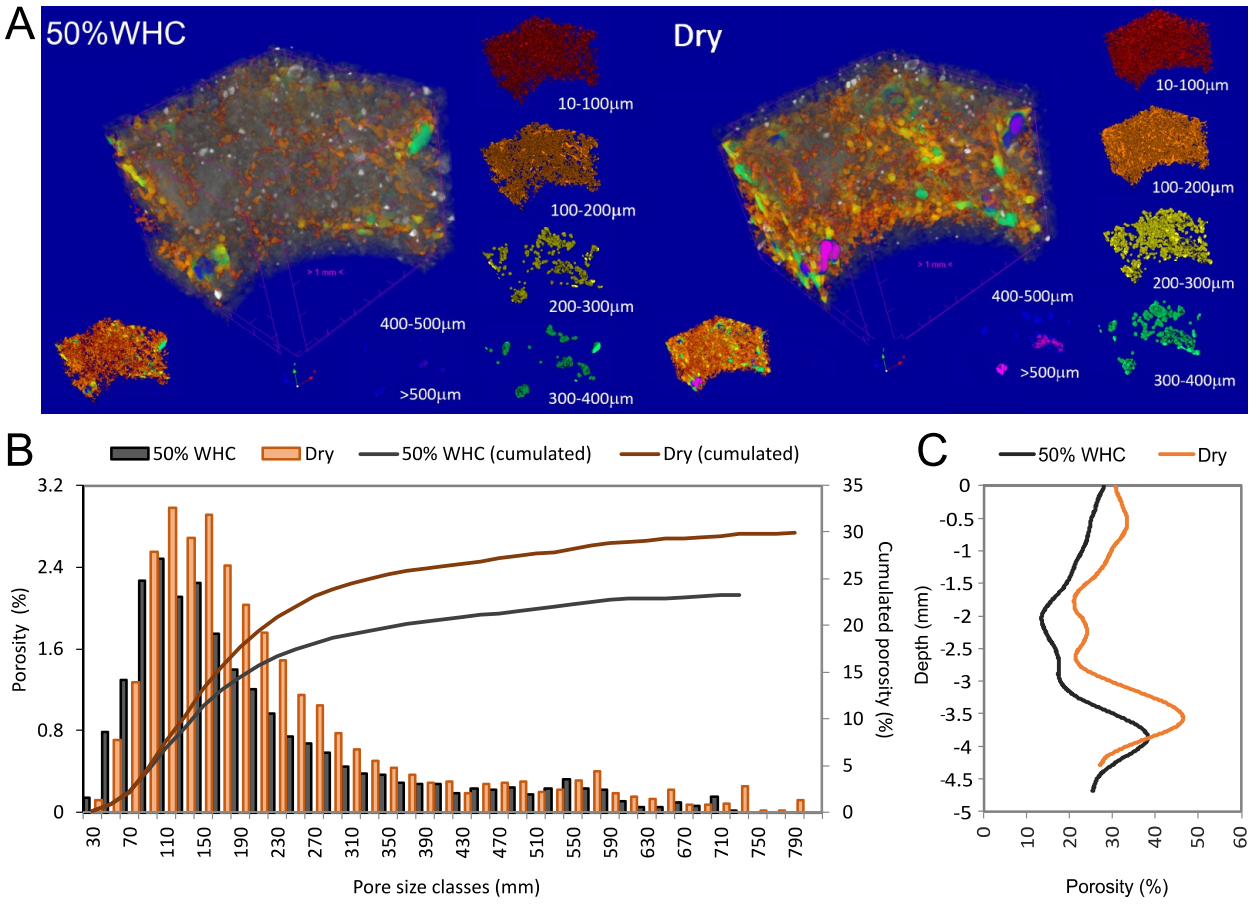

Figure 1. Structure and porosity of one biocrust sample at two hydration states: (A) 3D visualization of the biocrust pores at ~50% water holding capacity (WHC) corresponding to ~80% field capacity (FC) (left) and in a dry state (right), with pore volume size (µm) classified by color scale. Solid phase is shown in gray color, white spots are mineral grains inside the soil matrix; (B) pore size distribution at ~50% WHC and in a dry state; (C) vertical porosity profile of the crust sample at ~50% WHC and in a dry state.

over the course of desiccation. For each sensor type, at least five replicate measurements were conducted at different locations within biocrust samples. The sensors were moved in a vertical manner by means of a motorized micromanipulator (MM33, Märzhäuser Wetzlar GmbH & Co. KG, Wetzlar, Germany) to a depth of 5 mm. A typical desiccation cycle showed a linear decrease of the water content expressed as percentage of WHC (Figure S1), referring to the whole Petri dish serving as reference.

Statistical differences between the PL and the HL layers were analyzed for the microsensor profiles using the Mann−Whitney U test, since the data were not normally distributed (OriginLab Corporation, Northampton, Massachusetts, USA; Table S4). For more detailed information, see the Supplementary Methods.

Dynamic Chamber Measurements. The analysis of HONO and NO emissions was carried out in an air-flushed dynamic Teflon chamber.[18,20−23] HONO was detected spectrophotometrically, using a long path absorption photometer (LOPAP), whereas NO and NO_2 were analyzed with a gas chemiluminescence detector equipped with a blue light converter.[18,20,21,23] Measurements occurred at 25 °C in the dark to avoid photochemical reactions, and the samples were fully wetted to 100% WHC, placed in the chamber, and measured until complete desiccation. Further methodological information is provided in the Supplementary Methods.

RESULTS AND DISCUSSION

X-ray Microtomography. The pore-size distribution and vertical gradient of porosity of a biocrust sample was investigated at two hydration conditions, ~50 and 0% WHC, by means of X-ray microtomography (Figures 1 and S2). The obtained images showed that the locations of macropores did not change upon desiccation, whereas the overall volume of the crust sample decreased by 8% (from 1.64 to 1.51 cm^3; Figures 1A and S2). Total porosity increased from 23.3% at ~50% WHC to 29.9% in a dry state, maximum pore size diameters rose from 710 to 790 µm, and the mean pore size increased from 212 to 223 µm (Figure 1B). The main changes in pore diameter occurred between 70 and 350 µm (Figure 1B), while the vertical profile of porosity, measured along the entire biocrust sample, showed only minute changes (Figure 1C). Porosity was low between ~2−3 mm depth (~22% in a dry and <20% in a wet state), whereas above and below higher porosities were measured (with maximum values of ~45 and ~38% porosity in a dry and wet state, respectively). Local vertical profiles of porosity measured in a dry state showed great heterogeneity within the crust sample with the standard deviation of locally measured porosity values ranging from ~10% in the upper (until 2.2 mm depth) and lower (below 3.7 mm depth) part of the crust to ~30% between 2.2 and 3.7 mm depth (Figure. S3D). In this central layer, minimum and maximum porosity ranged from 0 to 100% (Figure. S3C), indicating presence of both solid aggregates and macropores.

https://doi.org/10.1021/acs.est.2c02207
Environ. Sci. Technol. 2022, 56, 11865−11877

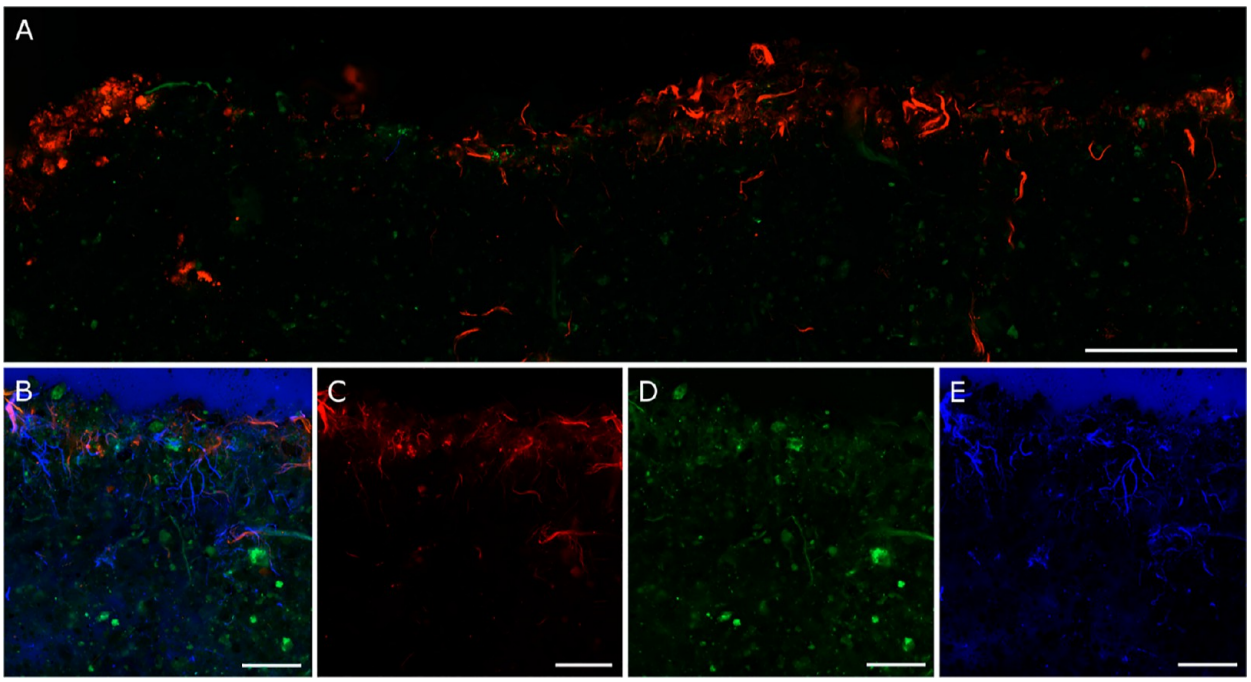

Figure 2. Fluorescence microcopy of biological soil crusts: (A) exemplary illustration of merged fluorescence micrographs of one cross-section of a cyanobacteria-dominated biocrust sample. The red channel shows photoautotrophic organisms; pedological features (e.g., sand grains, stones) are shown in green color. Scale represents 2.5 mm. (B,C,D,E) represent a subsection of a cyanobacteria-dominated biocrust. (B) Merged fluorescence image; (C) red channel, representing photoautotrophic organisms; (D) green channel, showing soil pedological features (e.g., sand grains, stones); and (E) blue channel, showing polysaccharides like chitin, cellulose, and the cyanobacterial extracellular polymeric substances (EPS). Scales represent 600 μm. For additional images, see Figure S4.

In total, only a general shrinkage of the solid phase occurred, which caused increased pore sizes within the biocrust along with a reduction of its overall volume. Consecutive microsensor profiling also showed a shrinkage of the biocrust, indicated by a retraction of the biocrust surface over the course of desiccation. Similarly, Rodríguez-Caballero et al.[55] showed an initial swelling of the biocrust surface upon hydration, followed by a shrinking during desiccation. They highlighted that the X-ray microtopography of the biocrust surface changed during hydration, with an increase in surface height and roughness (up to 0.24 and 0.20 mm, respectively) for lichen- and cyanobacteria-dominated biocrusts. There are several studies using X-ray microtomography to investigate the biocrust structure after disturbance,[56] to compare different ages of biocrusts,[57] or to show changes of the pore structure during crust succession.[58] Similar to our investigations on biocrust structure, the study of Couradeau et al.[59] showed that sand grains stayed in place, despite the fact that the microenvironment of EPS shrank during desiccation. This was mainly because the EPS sheaths did not strongly adhere to the sand grains. They could also show that EPS sheath material remained effectively hydrated while the surrounding soil pore regions were steadily drying. In another study, microbial extracellular polymeric substances (EPS) were described to alter soil water retention by reversible swelling of the cross-linked polymer matrix.[60]

Fluorescence Microscopy. Cross-sections revealed a distinctive layer of photoautotrophic organisms in the upper section of the biocrust, but the organisms were not evenly spread but rather concentrated in distinct clumps or hotspots (Figure 2 and S4A,B). In close-up images, a high variability of organism distribution at μm-scale became visible, and polysaccharides were closely associated with photoautotrophic organisms (Figure 2B−E). This was confirmed by occupancy maps of photoautotrophs and polysaccharides obtained by image segmentation with cross entropy thresholding (Figure 3A,B). The occupancy maps illustrate that the photoautotrophic organisms were mainly detected up to a depth of 0.4 mm (thereby defining the photoautotrophic layer, PL) with a notable horizontal variability (Figure 3A,C). A similar pattern was observed for complex polysaccharides, which were mainly concentrated in the uppermost part of the sample (Figure 3B,D). The Jaccard similarity index as a measure of co-occurrence of photoautotrophs and polysaccharides was highest in the PL (Figure 3E).

The heterogeneous distribution of complex polysaccharides, which also form EPS, suggests that they are involved in creating the heterogeneous micro-structure within biocrusts. Previous studies demonstrated that EPS protect microorganisms from ultraviolet radiation (UV) and desiccation, as the EPS matrix may contain UV shielding compounds like Scytonemin[61,62] and dries slower than its surroundings, thus enhancing their survival in water-deficient environments.[63,64] EPS are known to maintain hydration by water accumulation and regulation of water loss,[65−67] thus also contributing to N-cycling processes.[68] Furthermore, they mediate the adhesion to surfaces, allow an accumulation of nutrients and keep cells in close proximity, facilitating interactions.[63] In an earlier study it was shown that diazotrophic bacteria can be enriched in the EPS of a non-nitrogen-fixing cyanobacterium, thus influencing its N status.[69] Our X-ray CT imagery also displayed a strongly heterogeneous pore size structure (Figure 1A,B), which likely causes the heterogeneous colonization of the substrate.

The observed decreasing abundance of photoautotrophic organisms with depth (Figures 2 and 3) is in line with previous reports.[70,71] The distinctive PL in the upper part of the

https://doi.org/10.1021/acs.est.2c02207
Environ. Sci. Technol. 2022, 56, 11865−11877

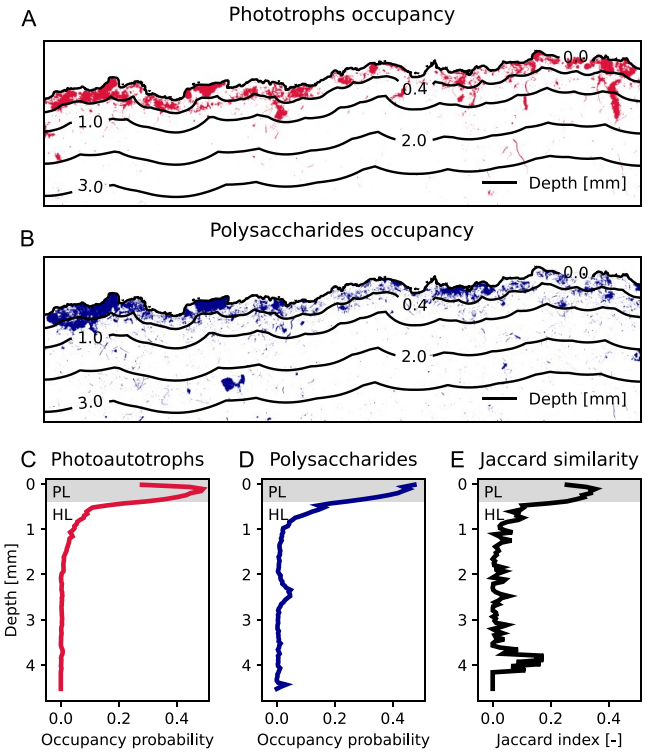

Figure 3. Depth profiles of a cyanobacteria-dominated biocrust cross-section. The red and blue channels of the fluorescence microscopy of the biocrust were used for occupancy maps of (A) photoautotrophic organisms (red) and (B) polysaccharides (blue) based on the minimum cross entropy thresholding. The colored patches indicate the occurrence and extent, the contour lines show the substrate depth. (C,D) The occupancy probability of both parameters were aggregated along soil depth in 50 μm steps. (E) Jaccard similarity index was used to quantify the degree of co-occurrences of photoautotrophs and polysaccharides. The grey shaded area in the profiles indicates the photoautotrophic layer (PL, depth ~0.4 mm), the area below is considered as the heterotrophic layer (HL, depth >0.4 mm).

biocrust (<0.4 mm depth) indicates the penetration depth of light, which leads to the high abundance of chlorophyll$_a$. Not only light, but also other factors play a role in the vertical distribution of the photoautotrophs, such as nutrients, water, temperature, and pore structure.[72] Biocrusts from Utah were colonized by the bundle-forming, filamentous cyanobacterium *Microcoleus vaginatus* Gomont, mainly occurring at 200−500 μm depth, whereas the network of sheaths extended to depths of 3−4 cm.[71] Also in our study, the polysaccharide concentration decreased somewhat less steeply with depth, but mainly reached to 1 mm depth.

For soils, it has been shown that they generally represent a heterogeneous and dynamic physicochemical environment. They are subject to temporal and spatial variation in the availability of water and nutrients, and the temperature fluctuates in spatially constrained pore spaces. These soil characteristics create microenvironments, differing in water volume, liquid−gas interfacial area, and nutrient availability, resulting in a heterogeneous, patchy distribution of microbes, for instance nitrifiers, in the soil.[73−86] Similarly, microbial populations are inhomogeneously distributed within biocrusts, mostly as a consequence of vertical gradients in light, oxygen, nutrients as well as water availability, soil properties (texture, pH), and temperature variations.[87,88] These reports are in accordance with our findings, as we observed a high heterogeneity in the spatial distribution of photoautotrophic organisms in the uppermost soil layer and a high heterogeneity in biogeochemical processes as explained below.

Biogeochemical Heterogeneity and Fluxes. Oxygen saturation, pH, and N compound concentrations (NO_2^-, NO_3^-, and NH_4^+) were measured using microsensors over the course of desiccation (Figures 4, 5 and S5). In Figure 4, vertical profiles at 100, 75, 50, and 25% WHC are presented, whereas in Figure 5 representative profiles assessed at hourly intervals over the course of a desiccation cycle are shown.

Generally, the microsensor measurements revealed that profiles taken at different locations within biocrust samples differed to a large extent, irrespective of the measured parameter.

At full WHC, oxygen contents showed high spatial heterogeneity, displaying steeply declining oxygen contents with increasing depth, reaching a mean saturation minimum of 18 ± 22% at 0.8 mm depth. Towards deeper layers the values increased slowly again, reaching a mean saturation maximum of 54 ± 27% at 4.2 mm depth (Figure 4A). Already at 75% WHC, the mean saturation value had increased to an overall value of ~91 ± 2% with no major differences along depth, indicating an oxygenation of the entire sample that persisted during the subsequent desiccation (Figure 4A and 5A−C). The O_2-sensors showed lowest O_2 saturation at high WHC, likely due to the respiration activity of photoautotrophic and heterotrophic microorganisms in combination with the increased diffusion resistance of water as compared to air-filled pores (Figure 4A, 5A−C and 6A). Anoxic conditions in soil occur when the oxygen consumption rate exceeds the oxygen production/transport rate. Especially after hydration, the solubilization of nutrients and the onset of metabolic activity after desiccation stimulate respiration and subsequently result in such anoxic regions.[89] Our results suggest that the microbial respiration was sufficient to create anoxic regions, even in the upper region close to the interface with the atmosphere. This was similarly observed in earlier studies, where anoxic areas occurred from the surface to several millimeters depth in fully saturated biocrusts.[71] Such events of full water saturation with anoxic conditions do not occur frequently in drylands, but mesoclimate data assessed during the BIOTA project (www.biota-africa.org) and during measurements of ourselves (B. Weber, unpublished) show that daily precipitation reaching 10−20 mm normally occurs on several occasions per year. During these occasions, we expect at least nearly full water saturation to be reached over short time-spans. As soil dries, gaseous diffusion is facilitated and allows oxygenation of the soil.[76] We observed that both the photoautotrophic and heterotrophic layers became fully oxygenated when the biocrust sample dried to ~70% WHC (equivalent to a water content of 0.09 g * g^{-1}; Figure 6). However, in this context it has to be considered that, because of the measurement conditions (darkness), no photosynthesis occurred. In former studies, photosynthesis in illuminated biocrusts recovered within minutes after hydration, resulting in the formation of an oxygen-supersaturated zone close to the surface and anoxic zones at 1−3 mm depth.[90]

The microsensor measurements also revealed not only vertical but also horizontal microscale heterogeneity. Spatially restricted areas and limited periods of oxygen-limited conditions over the course of desiccation (Figure 4A and 5A−C) are likely caused by the patchy distribution of microbial cells and EPS (Figure 2) causing variations in

https://doi.org/10.1021/acs.est.2c02207
Environ. Sci. Technol. 2022, 56, 11865−11877

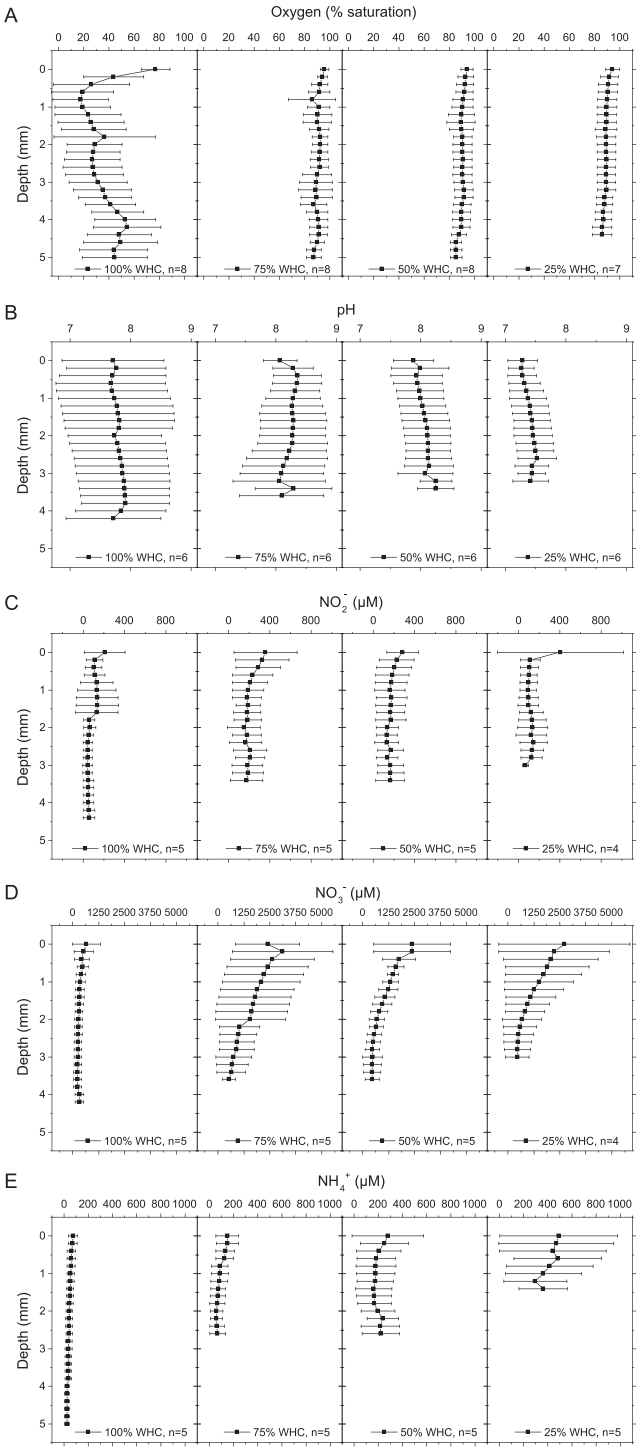

Figure 4. Microsensor profiles of biocrusts assessed at 100, 75, 50 and 25% water holding capacity (WHC) at different locations: (A) oxygen saturation [%]; (B) pH; (C) nitrite (NO_2^-) concentration [μM]; (D) nitrate (NO_3^-) concentration [μM]; (E) ammonium (NH_4^+) concentration [μM]. Error bars indicate standard deviation. For additional information on locations, please refer to Table S3. Locations without changes during desiccation are not included.

oxygen production/consumption and transport. Previous studies of desert biocrusts have also shown that respiration in cyanobacterial crusts started within minutes upon hydration, and, in line with our observations, it was concluded that disparate chemical microsites had formed,[71,90,91] which were also suitable for anaerobic processes, such as anaerobic methanogenesis in crusts from the Negev Desert[92] and denitrification in crusts from Oman.[10]

Average pH values increased from 100 to 75% WHC with a mean maximum of 8.4 ± 0.4 at 0.4 mm depth. During subsequent desiccation, the mean values decreased again, maximum values shifted towards deeper layers (~2−3 mm depth), and at 25% WHC the near-surface pH (7.2 ± 0.3) was lower than the initial value at full WHC (7.7. ± 0.8; Figure 4B). During individual microsensor measurements, the pH values ranged between ~6.5 and ~9 at different locations and desiccation stages (Figure 5D−F and S5). Whereas in some locations pH values decreased considerably over the course of desiccation (from ~9.0 to ~6.9; Figure 5D), in other spots nearly no changes in pH were observed over the course of desiccation (Figure 5F). We detected locations with high pH values at the beginning of the measurement that decreased over the course of desiccation, which may be caused by chemical reactions and biological processes. In former measurements, variable pH values were reported for bulk samples of different dark cyanobacteria-dominated biocrusts from the Succulent Karoo and Cyprus, ranging from 6.8 to 8.0 and 6.8 to 7.3, respectively.[18,20]

Mean NO_2^- concentrations revealed an increase and a subsequent decrease from 86 μM at 100% WHC to 212, 174, and 133 μM at 75, 50, and 25% WHC, respectively (Figure 4C). At 100% WHC, highest mean NO_2^- concentrations of 136 μM were reached at 1−1.6 mm depth, whereas subsequently the highest mean values occurred at the surface. Lowest standard deviations were observed at 100% WHC at 1.8 mm depth and below, whereas the highest value occurred at the surface at 25% WHC. Individual measurements showed large variation, as some of them were characterized by increasing concentrations at specific depths (Figure 5G), others showed increased concentrations towards the biocrust surface, with a stable pattern throughout the desiccation process (Figure 5H), and a third group displayed no major changes in deeper layers and only somewhat higher concentrations close to the surface (Figure 5I). The initial increase in NO_2^- was probably due to the onset of spatially localized microbial activity upon hydration. Recent work has shown that soil bacteria respond within hours to days to an increase in soil water availability after prolonged drought.[93−95] The quick microbial response is associated with CO_2 emissions[93] and an increase in transcript copies of bacterial *rpoB* genes, encoding bacterial RNA polymerase, indicating resumption of transcriptional activity.[96]

Average NO_3^- concentrations were lowest at full WHC (337 ± 108 μM) and highest at 75% WHC (1572 ± 766 μM) (Figure 4D). With progressing desiccation, there was a slight reduction in maximum values, and generally mean concentrations were high close to the surface and showed a strong decrease towards deeper strata. Such high surface values were also observed in individual measurements, but only in one representative sample, this stratification lasted until desiccation (Figure 5K), whereas in another sample a stratification dissolved below 70% WHC (Figure 5J). Also for NO_3^- there were measurements where no major changes were observed along desiccation (Figure 5L).

Ammonium concentrations were lowest at full WHC and increased over the course of desiccation, accompanied by increasing standard deviations (Figure 4E). Generally, the highest concentrations occurred close to the surface, but at

https://doi.org/10.1021/acs.est.2c02207
Environ. Sci. Technol. 2022, 56, 11865−11877

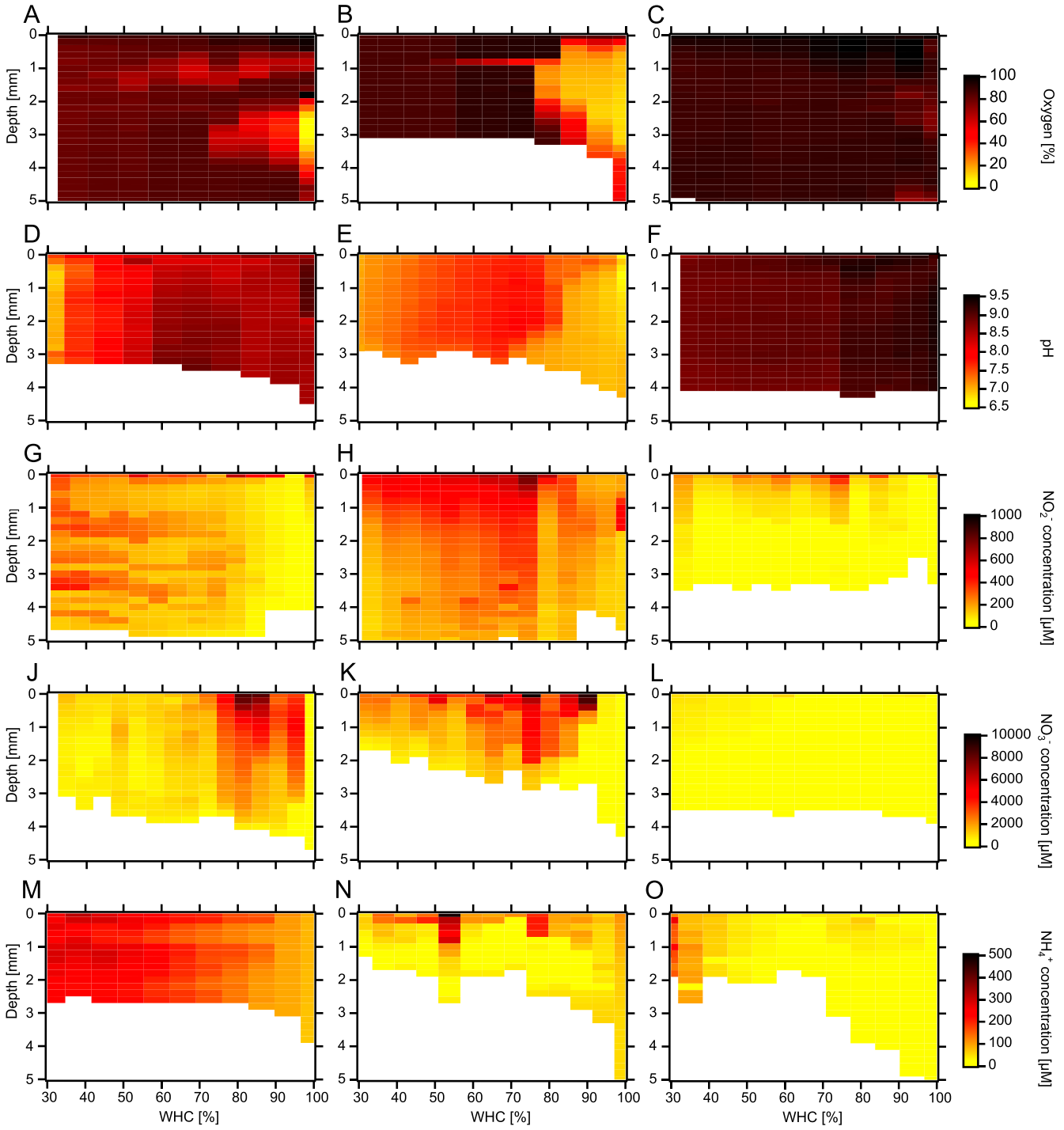

Figure 5. Vertical microsensor profiles (up to a depth of 5 mm) of biocrusts assessed at varying water holding capacity (WHC). (A–C) Oxygen saturation [%], (D–F) pH, (G–I) nitrite (NO_2^-) concentration [μM], (J–L), nitrate (NO_3^-) concentration [μM], (M–O) ammonium (NH_4^+) concentration [μM] in representative biocrust profiles (with the three columns showing measurements at three different locations/puncture sites, reflecting the range of variability) over the course of drying. Profiles were performed at hourly intervals and WHC refers to the whole Petri dish. Additional information on locations measured with different sensor types is given in Table S3. Further measurements are shown in Figure S5.

50% WHC slightly increased concentrations were also observed at ~2.4 mm depth. In some individual sensor measurements, the increasing ammonium concentrations along desiccation could be nicely observed (Figure 5M), whereas in others increased values occurred mainly towards the surface, but were otherwise fairly stable (Figure 5N). In other measurements, increased values were only observed towards the end of desiccation (Figure 5O).

Generally, soil water content has been identified as the main variable that controls the pore space, hence shapes diffusion of oxygen and other nutrients.[97] The small-scale structural heterogeneity of the substrate and its pore space, which has been observed during X-ray microtomography, thus explains the variability of oxygen and nutrient contents at the microscale. This availability of oxygen and nutrients to microorganisms has been shown to influence the rates and patterns

https://doi.org/10.1021/acs.est.2c02207
Environ. Sci. Technol. 2022, 56, 11865−11877

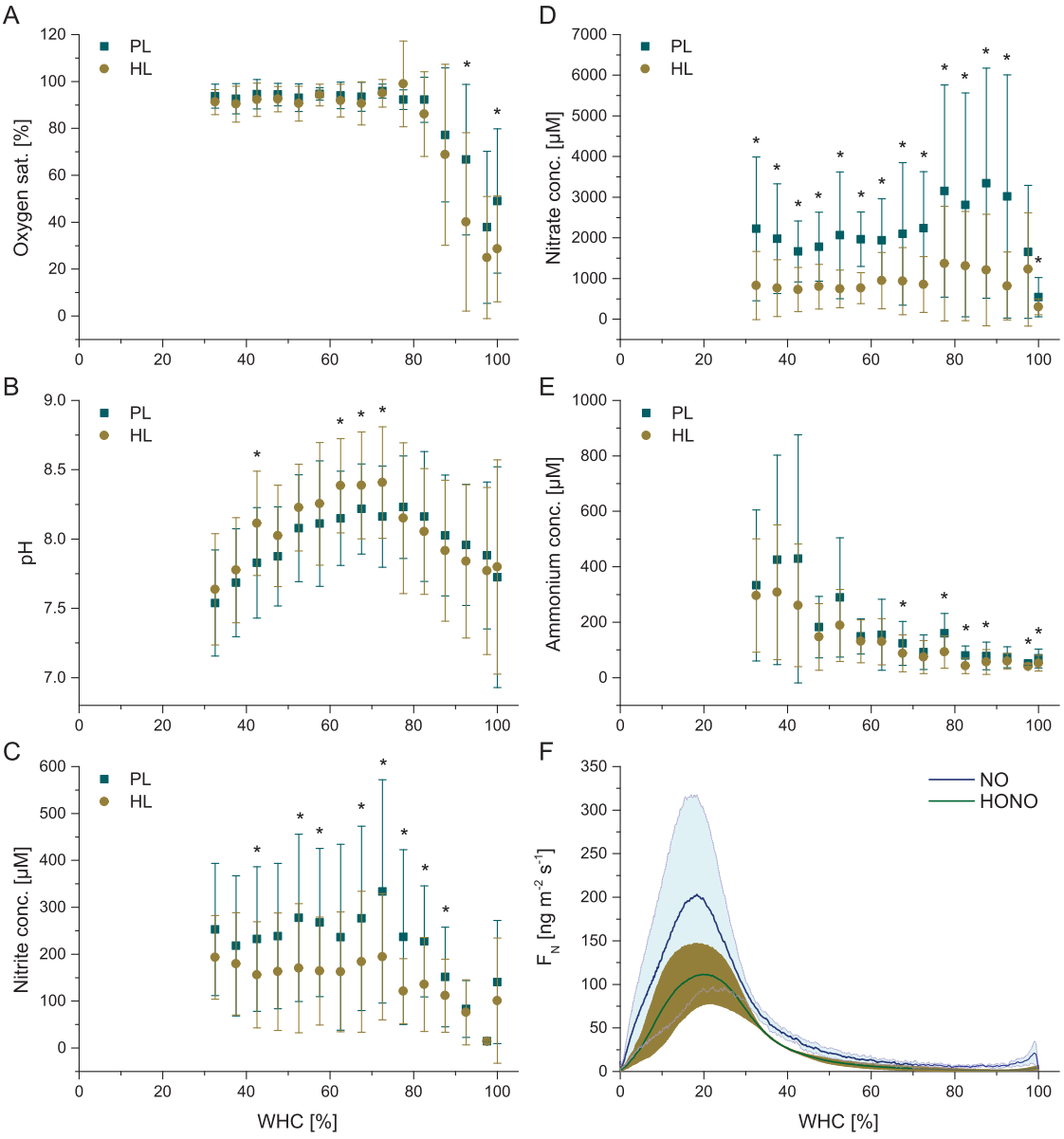

Figure 6. Mean microsensor readings in the photoautotrophic (PL) and heterotrophic layer (HL) and HONO- and NO emissions of biocrust samples as related to the water holding capacity (WHC). (A) Oxygen saturation, (B) pH, (C) nitrite (NO_2^-), (D) nitrate (NO_3^-), (E) ammonium (NH_4^+) content. Measurements were conducted on biocrusts over the course of desiccation and contain several replicates (O_2: 8; pH: 6; NO_2^-/NO_3^-/NH_4^+: 5). Photoautotrophic layer (PL) covers 0−400 μm depth (200 μm steps obtained by vertical profiles), the heterotrophic layer (HL) starts at 600 μm until the maximum measurement depth; WHC covers the indicated values ± 2.5% (see Methods Section for details). Microsensor profiles without changes during desiccation are not included. Asterisks show significant differences between PL and HL (Statistical results are shown in Table S4) and error bars indicate standard deviation. (F) Average reactive nitrogen emission flux (F_N) of NO and HONO as a function of water holding capacity (WHC). Lines indicate the mean fluxes and shaded areas the standard deviation.

of biogeochemical processes, which could cause emissions of CO_2, N_2O, and CH_4 from soil aggregates.[80,98−100] During desiccation, we observed that only the concentration of ammonium showed an increase, whereas that of NO_2^- and NO_3^- remained fairly stable, indicating a conversion of both nitrogen species. An explanation for the NO_2^- loss could be its emission as HONO or NO from the biocrust.[20] The loss of NO_3^- could be due to denitrification.

Microsensor Data Related to Dynamic Chamber Measurements. Although the microsensor technique allowed measurements only until 30% WHC (but not below), these data still could be related to online chamber flux measurements that showed increasing N_r emissions at 30% WHC (Figure 6). Oxygen saturation values of fully wetted samples increased strongly until 80% WHC, with higher values in the PL as compared to the HL, and stayed similarly high until desiccation (Figure 6A). This was different for the pH, which first increased until a WHC of ∼70% and then showed a strong decrease again, reaching a mean pH of ∼7.6 (Figure 6B). This final decrease of pH coincided with increasing HONO and NO emissions (Figure 6F). This is in line with the mechanistic soil model predictions of Kim and Or,[100] who suggested that changes in aqueous film thickness and a local decrease in pH during desiccation drives the emission of HONO.[100,101] The model prediction also supports our findings by demonstrating that mean water content and bulk soil pH

https://doi.org/10.1021/acs.est.2c02207
Environ. Sci. Technol. 2022, 56, 11865−11877

values may not capture the nuances at microscale associated with efflux patterns, like the HONO emissions from alkaline soils or the concurrent emissions of NH_3 and HONO during desiccation cycles.[100]

Also the mean NO_2^- concentrations increased until ∼70% WHC (PL up to 350 μM and HL up to 200 μM), which was followed by a slight decrease in the PL and constant values in the HL (Figure 6C). Mean NO_3^- concentrations were highest at high water contents of ∼80−90% WHC (PL up to 3500 μM and HL up to 1500 μM) and subsequently they stabilized at values around 2000 μM in the PL and around 750 μM in the HL (Figure 6D). For both NO_2^- and NO_3^- the values were mostly significantly higher in the PL as compared to the HL (Figure 6C,D). Mean ammonium concentrations increased with progressing desiccation accompanied by increasing standard deviations (Figure 6E). Mean HONO and NO values showed a maximum flux of 112.57 ± 113.32 ng m^{-2} s^{-1} HONO−N and 205.34 ± 34.27 ng m^{-2} s^{-1} NO−N, respectively, at ∼20% WHC (Figure 6F). Thus, the concentrations of N-compounds were also highly variable in space and time, but generally the lowest values occurred at full WHC and increased towards 75% WHC with subsequently decreasing NO_2^-, increasing ammonium, and stable NO_3^- values (Figure 6C−E). This fits to the observation that lower pH values are associated with decreased rates of ammonia oxidation (AO), leading to a decrease in NO_2^- at lower WHC.[102] Interestingly, concentrations of NO_3^- were generally higher than those of NO_2^-, which is in line with NO_2^- and NO_3^- contents obtained for complete biocrust samples.[32] The highly variable measurement results indicate that biotic processes, such as nitrification and denitrification, with NO_2^- as an intermediate product and precursor of HONO, are spatially restricted. Microsites with high reaction rates compared to the surrounding area have been observed in soil, where a nonhomogeneous distribution of denitrification activity has been identified.[103,104] In future studies, it would be desirable to investigate the same samples with different techniques, for example X-ray CT and fluorescence microscopy, in order to have a direct link between structural and organismic composition, or fluorescence microscopy and microsensor measurements, in order to link organismic and nutrient composition.

Overall, our study revealed that the biocrust substrate structure consisted of a stable mix of pore size classes, the distribution of organisms was patchy, and the ion concentrations occurred in strongly heterogeneous patterns. Our results suggest that the highly variable biocrust structure allows the formation of spatially separated microhabitats, where different, highly dynamic and even contradictory soil N transformations occur simultaneously within millimeter distances during drying. This knowledge needs to be considered in future global change and land management scenarios.

■ ASSOCIATED CONTENT

Supporting Information

The Supporting Information is available free of charge at https://pubs.acs.org/doi/10.1021/acs.est.2c02207.

Methods (Sampling, X-ray microtomography, Fluorescence microscopy, LIX sensors, Dynamic chamber measurements), Water holding capacity (%) of a biocrust (Figure S1), X-ray microtomography images of a biocrust sample (Figure S2), Porosity profiles of a biocrust sample (Figure S3), Fluorescence images showing photoautotrophic organisms and polysaccharides (Figure S4), Microsensor profiles of oxygen saturation, pH, and N compound concentrations (Figure S5), Information on X-ray micro-CT (Table S1-S2), Information on microsensor measurements (puncture sites, date of measurement, Table S3), Results of statistical analysis for microsensor measurements (Table S4) (PDF)

■ AUTHOR INFORMATION

Corresponding Authors

Alexandra Maria Kratz − *Multiphase Chemistry Department, Max Planck Institute for Chemistry, Mainz 55128, Germany;* orcid.org/0000-0003-3309-312X; Email: a.kratz@mpic.de

Bettina Weber − *Multiphase Chemistry Department, Max Planck Institute for Chemistry, Mainz 55128, Germany; Institute of Biology, Division of Plant Sciences, University of Graz, Graz 8010, Austria;* orcid.org/0000-0002-5453-3967; Email: b.weber@mpic.de

Authors

Stefanie Maier − *Multiphase Chemistry Department, Max Planck Institute for Chemistry, Mainz 55128, Germany; Institute of Biology, Division of Plant Sciences, University of Graz, Graz 8010, Austria*

Jens Weber − *Multiphase Chemistry Department, Max Planck Institute for Chemistry, Mainz 55128, Germany; Institute of Biology, Division of Plant Sciences, University of Graz, Graz 8010, Austria*

Minsu Kim − *Institute of Biology, Division of Plant Sciences, University of Graz, Graz 8010, Austria*

Giacomo Mele − *Institute for Agriculture and Forestry in the Mediterranean, National Council of Research, 80055 Portici, Italy*

Laura Gargiulo − *Institute for Agriculture and Forestry in the Mediterranean, National Council of Research, 80055 Portici, Italy*

Anna Lena Leifke − *Multiphase Chemistry Department, Max Planck Institute for Chemistry, Mainz 55128, Germany*

Maria Prass − *Multiphase Chemistry Department, Max Planck Institute for Chemistry, Mainz 55128, Germany*

Raeid M. M. Abed − *College of Science, Biology Department, Sultan Qaboos University, Seeb 123, Sultanate of Oman*

Yafang Cheng − *Multiphase Chemistry Department, Max Planck Institute for Chemistry, Mainz 55128, Germany;* orcid.org/0000-0003-4912-9879

Hang Su − *Multiphase Chemistry Department, Max Planck Institute for Chemistry, Mainz 55128, Germany;* orcid.org/0000-0003-4889-1669

Ulrich Pöschl − *Multiphase Chemistry Department, Max Planck Institute for Chemistry, Mainz 55128, Germany;* orcid.org/0000-0003-1412-3557

Complete contact information is available at: https://pubs.acs.org/10.1021/acs.est.2c02207

Author Contributions

⊥A.M.K., S.M., and J.W. contributed equally to this work

Funding

Open access funded by Max Planck Society.

Notes

The authors declare no competing financial interest.

■ ACKNOWLEDGMENTS

Research described within this paper was supported by the Max Planck Graduate Center with the Johannes Gutenberg University, Mainz (MPGC) and has been funded and supported by the Max Planck Society (Nobel Laureate Fellowship to B.W.). We would like to acknowledge the support by the Hanse-Wissenschaftskolleg (HWK; Institute for Advanced Study, Germany) with the study group of Raeid M.M. Abed. We would like to thank Dirk de Beer and his technician team for offering microsensor workshops (usage and production) and providing laboratory facilities. Weather data of BIOTA Southern Africa, station Soebatsfontein, as on May 27, 2022 (www.biota-africa.org), has been used for interpretation of the data and is greatly acknowledged.

■ REFERENCES

(1) Belnap, J.; Weber, B.; Büdel, B., Biological soil crusts as an organizing principle in drylands. In *Biological soil crusts: An organizing principle in drylands. Ecological Studies 226.*, Weber, B.; Büdel, B.; Belnap, J., Eds. Springer International Publishing: Cham, 2016; pp 3-13.

(2) Bowker, M. A.; Reed, S. C.; Maestre, F. T.; Eldridge, D. J. Biocrusts: the living skin of the earth. *Plant Soil* **2018**, *429*, 1−7.

(3) Maestre, F. T.; Bowker, M. A.; Cantón, Y.; Castillo-Monroy, A. P.; Cortina, J.; Escolar, C.; Escudero, A.; Lázaro, R.; Martínez, I. Ecology and functional roles of biological soil crusts in semi-arid ecosystems of Spain. *J. Arid Environ.* **2011**, *75*, 1282−1291.

(4) Maier, S.; Tamm, A.; Wu, D.; Caesar, J.; Grube, M.; Weber, B. Photoautotrophic organisms control microbial abundance, diversity, and physiology in different types of biological soil crusts. *ISME J.* **2018**, *12*, 1032−1046.

(5) Rodriguez-Caballero, E.; Belnap, J.; Büdel, B.; Crutzen, P. J.; Andreae, M. O.; Pöschl, U.; Weber, B. Dryland photoautotrophic soil surface communities endangered by global change. *Nat. Geosci.* **2018**, *11*, 185−189.

(6) Elbert, W.; Weber, B.; Burrows, S.; Steinkamp, J.; Büdel, B.; Andreae, M. O.; Pöschl, U. Contribution of cryptogamic covers to the global cycles of carbon and nitrogen. *Nat. Geosci.* **2012**, *5*, 459−462.

(7) Barger, N. N.; Weber, B.; Garcia-Pichel, F.; Zaady, E.; Belnap, J., Patterns and controls on nitrogen cycling of biological soil crusts. In *Biological soil crusts: An organizing principle in drylands*, Weber, B.; Büdel, B.; Belnap, J., Eds. Springer International Publishing: Cham, 2016; pp 257-285.

(8) Sancho, L. G.; Belnap, J.; Colesie, C.; Raggio, J.; Weber, B., Carbon budgets of biological soil crusts at micro-, meso-, and global scales. In *Biological soil crusts: An organizing principle in drylands*, Weber, B.; Büdel, B.; Belnap, J., Eds. Springer International Publishing: Cham, 2016; pp 287-304.

(9) Housman, D. C.; Powers, H. H.; Collins, A. D.; Belnap, J. Carbon and nitrogen fixation differ between successional stages of biological soil crusts in the Colorado Plateau and Chihuahuan Desert. *J. Arid Environ.* **2006**, *66*, 620−634.

(10) Abed, R. M. M.; Lam, P.; de Beer, D.; Stief, P. High rates of denitrification and nitrous oxide emission in arid biological soil crusts from the Sultanate of Oman. *ISME J.* **2013**, *7*, 1862−1875.

(11) Lenhart, K.; Weber, B.; Elbert, W.; Steinkamp, J.; Clough, T.; Crutzen, P.; Pöschl, U.; Keppler, F. Nitrous oxide and methane emissions from cryptogamic covers. *GCB* **2015**, *21*, 3889−3900.

(12) McCalley, C. K.; Sparks, J. P. Abiotic gas formation drives nitrogen loss from a desert ecosystem. *Science* **2009**, *326*, 837−840.

(13) McCalley, C. K.; Sparks, J. P. Controls over nitric oxide and ammonia emissions from Mojave Desert soils. *Oecologia* **2008**, *156*, 871−881.

(14) Kubota, M.; Asami, T. Source of nitrous acid volatilized from upland soils. *Soil Sci. Plant Nutr.* **1985**, *31*, 35−42.

(15) Maljanen, M.; Yli-Pirilä, P.; Hytönen, J.; Joutsensaari, J.; Martikainen, P. J. Acidic northern soils as sources of atmospheric nitrous acid (HONO). *Soil Biol. Biochem.* **2013**, *67*, 94−97.

(16) Mamtimin, B.; Meixner, F. X.; Behrendt, T.; Badawy, M.; Wagner, T. The contribution of soil biogenic NO and HONO emissions from a managed hyperarid ecosystem to the regional NO_x emissions during growing season. *Atmos. Chem. Phys.* **2016**, *16*, 10175−10194.

(17) Meusel, H.; Kuhn, U.; Reiffs, A.; Mallik, C.; Harder, H.; Martinez, M.; Schuladen, J.; Bohn, B.; Parchatka, U.; Crowley, J. N.; Fischer, H.; Tomsche, L.; Novelli, A.; Hoffmann, T.; Janssen, R. H. H.; Hartogensis, O.; Pikridas, M.; Vrekoussis, M.; Bourtsoukidis, E.; Weber, B.; Lelieveld, J.; Williams, J.; Pöschl, U.; Cheng, Y.; Su, H. Daytime formation of nitrous acid at a coastal remote site in Cyprus indicating a common ground source of atmospheric HONO and NO. *Atmos. Chem. Phys.* **2016**, *16*, 14475−14493.

(18) Meusel, H.; Tamm, A.; Kuhn, U.; Wu, D.; Leifke, A. L.; Fiedler, S.; Ruckteschler, N.; Yordanova, P.; Lang-Yona, N.; Pöhlker, M.; Lelieveld, J.; Hoffmann, T.; Pöschl, U.; Su, H.; Weber, B.; Cheng, Y. Emission of nitrous acid from soil and biological soil crusts represents an important source of HONO in the remote atmosphere in Cyprus. *Atmos. Chem. Phys.* **2018**, *18*, 799−813.

(19) Barger, N. N.; Belnap, J.; Ojima, D. S.; Mosier, A. NO Gas Loss from Biologically Crusted Soils in Canyonlands National Park, Utah. *Biogeochemistry* **2005**, *75*, 373−391.

(20) Weber, B.; Wu, D.; Tamm, A.; Ruckteschler, N.; Rodríguez-Caballero, E.; Steinkamp, J.; Meusel, H.; Elbert, W.; Behrendt, T.; Sörgel, M.; Cheng, Y.; Crutzen, P. J.; Su, H.; Pöschl, U. Biological soil crusts accelerate the nitrogen cycle through large NO and HONO emissions in drylands. *Proc. Natl. Acad. Sci. U. S. A.* **2015**, *112*, 15384−15389.

(21) Oswald, R.; Behrendt, T.; Ermel, M.; Wu, D.; Su, H.; Cheng, Y.; Breuninger, C.; Moravek, A.; Mougin, E.; Delon, C.; Loubet, B.; Pommerening-Röser, A.; Sörgel, M.; Pöschl, U.; Hoffmann, T.; Andreae, M. O.; Meixner, F. X.; Trebs, I. HONO emissions from soil bacteria as a major source of atmospheric reactive nitrogen. *Science* **2013**, *341*, 1233−1235.

(22) Oswald, R.; Ermel, M.; Hens, K.; Novelli, A.; Ouwersloot, H. G.; Paasonen, P.; Petäjä, T.; Sipilä, M.; Keronen, P.; Bäck, J.; Königstedt, R.; Hosaynali Beygi, Z.; Fischer, H.; Bohn, B.; Kubistin, D.; Harder, H.; Martinez, M.; Williams, J.; Hoffmann, T.; Trebs, I.; Sörgel, M. A comparison of HONO budgets for two measurement heights at a field station within the boreal forest in Finland. *Atmos. Chem. Phys.* **2015**, *15*, 799−813.

(23) Su, H.; Cheng, Y. F.; Oswald, R.; Behrendt, T.; Trebs, I.; Meixner, F. X.; Andreae, M. O.; Cheng, P.; Zhang, Y.; Pöschl, U. Soil nitrite as a source of atmospheric HONO and OH radicals. *Science* **2011**, *333*, 1616−1618.

(24) Ciais, P.; Sabine, C.; Bala, G.; Bopp, L.; Brovkin, V.; Canadell, J.; Chhabra, A.; DeFries, R.; Galloway, J.; Heimann, M.; Jones, C.; Le Quéré, C.; Myneni, R. B.; Piao, S.; Thornton, P., Carbon and other biogeochemical cycles. In *Climate Change 2013 − The Physical Science Basis: Working Group I Contribution to the Fifth Assessment Report of the Intergovernmental Panel on Climate Change*, Stocker, T. F.; Qin, D.; Plattner, G.-K.; Tignor, M.; Allen, S. K.; Boschung, J.; Nauels, A.; Xia, Y.; Bex, V.; Midgley, P. M., Eds. Cambridge University Press: Cambridge, 2013; pp 465-570.

(25) Shoemaker, J. K.; Schrag, D. P.; Molina, M. J.; Ramanathan, V. What role for short-lived climate pollutants in mitigation policy? *Science* **2013**, *342*, 1323−1324.

(26) Chameides, W. L.; Fehsenfeld, F.; Rodgers, M. O.; Cardelino, C.; Martinez, J.; Parrish, D.; Lonneman, W.; Lawson, D. R.; Rasmussen, R. A.; Zimmerman, P.; Greenberg, J.; Mlddleton, P.; Wang, T. Ozone precursor relationships in the ambient atmosphere. *J. Geophys. Res. Atmos.* **1992**, *97*, 6037−6055.

(27) Crutzen, P. J. The Role of NO and NO2 in the Chemistry of the Troposphere and Stratosphere. *Annu. Rev. Earth Planet. Sci.* **1979**, *7*, 443−472.
(28) Lammel, G.; Graßl, H. Greenhouse effect of NOX. *Environ. Sci. Pollut. Res. Int.* **1995**, *2*, 40−45.
(29) Monks, P. S.; Granier, C.; Fuzzi, S.; Stohl, A.; Williams, M. L.; Akimoto, H.; Amann, M.; Baklanov, A.; Baltensperger, U.; Bey, I.; Blake, N.; Blake, R. S.; Carslaw, K.; Cooper, O. R.; Dentener, F.; Fowler, D.; Fragkou, E.; Frost, G. J.; Generoso, S.; Ginoux, P.; Grewe, V.; Guenther, A.; Hansson, H. C.; Henne, S.; Hjorth, J.; Hofzumahaus, A.; Huntrieser, H.; Isaksen, I. S. A.; Jenkin, M. E.; Kaiser, J.; Kanakidou, M.; Klimont, Z.; Kulmala, M.; Laj, P.; Lawrence, M. G.; Lee, J. D.; Liousse, C.; Maione, M.; McFiggans, G.; Metzger, A.; Mieville, A.; Moussiopoulos, N.; Orlando, J. J.; O'Dowd, C. D.; Palmer, P. I.; Parrish, D. D.; Petzold, A.; Platt, U.; Pöschl, U.; Prévôt, A. S. H.; Reeves, C. E.; Reimann, S.; Rudich, Y.; Sellegri, K.; Steinbrecher, R.; Simpson, D.; ten Brink, H.; Theloke, J.; van der Werf, G. R.; Vautard, R.; Vestreng, V.; Vlachokostas, C.; von Glasow, R. Atmospheric composition change − global and regional air quality. *Atmos. Environ.* **2009**, *43*, 5268−5350.
(30) Seinfeld, J. H.; Pandis, S. N., *Atmospheric Chemistry and Physics: From Air Pollution to Climate Change*. 2nd ed.; John Wiley & Sons: Hoboken, NJ, 2006; p 1203.
(31) Crutzen, P. J.; Zimmermann, P. H. The changing photochemistry of the troposphere. *Tellus Dyn. Meteorol. Oceanogr.* **1991**, *43*, 136−151.
(32) Maier, S.; Kratz, A. M.; Weber, J.; Prass, M.; Liu, F.; Clark, A. T.; Abed, R. M. M.; Su, H.; Cheng, Y.; Eickhorst, T.; Fiedler, S.; Pöschl, U.; Weber, B. Water-driven microbial nitrogen transformations in biological soil crusts causing atmospheric nitrous acid and nitric oxide emissions. *ISME J.* **2021**, *16* (4), 1012−1024.
(33) Sedlacek, C. J.; Giguere, A. T.; Dobie, M. D.; Mellbye, B. L.; Ferrell, R. V.; Woebken, D.; Sayavedra-Soto, L. A.; Bottomley, P. J.; Daims, H.; Wagner, M.; Pjevac, P. Transcriptomic response of *Nitrosomonas europaea* transitioned from ammonia- to oxygen-limited steady-state growth. *mSystems* **2020**, *5* (1), DOI: 10.1128/mSystems.00562-19
(34) Caranto, J. D.; Lancaster, K. M. Nitric oxide is an obligate bacterial nitrification intermediate produced by hydroxylamine oxidoreductase. *Proc. Natl. Acad. Sci. U. S. A.* **2017**, *114*, 8217−8222.
(35) Meixner, F. X.; Yang, W. X., Biogenic emissions of nitric oxide and nitrous oxide from arid and semi-arid land. In *Dryland Ecohydrology*, D'Odorico, P.; Porporato, A., Eds. Springer Netherlands: Dordrecht, 2006; pp 233-255.
(36) Wu, D.; Horn, M. A.; Behrendt, T.; Müller, S.; Li, J.; Cole, J. A.; Xie, B.; Ju, X.; Li, G.; Ermel, M.; Oswald, R.; Fröhlich-Nowoisky, J.; Hoor, P.; Hu, C.; Liu, M.; Andreae, M. O.; Pöschl, U.; Cheng, Y.; Su, H.; Trebs, I.; Weber, B.; Sörgel, M. Soil HONO emissions at high moisture content are driven by microbial nitrate reduction to nitrite: tackling the HONO puzzle. *ISME J.* **2019**, *13*, 1688−1699.
(37) Weber, B.; Tamm, A.; Maier, S.; Rodríguez-Caballero, E. Biological soil crusts of the Succulent Karoo: a review. *Afr. J. Range Forage Sci.* **2018**, *35*, 335−350.
(38) Butterbach-Bahl, K.; Baggs, E. M.; Dannenmann, M.; Kiese, R.; Zechmeister-Boltenstern, S. Nitrous oxide emissions from soils: how well do we understand the processes and their controls? *Philos. Trans. R. Soc., B* **2013**, *368*(1621), DOI: 10.1098/rstb.2013.0122.
(39) Cowan, N. J.; Norman, P.; Famulari, D.; Levy, P. E.; Reay, D. S.; Skiba, U. M. Spatial variability and hotspots of soil N_20 fluxes from intensively grazed grassland. *Biogeosciences* **2015**, *12*, 1585−1596.
(40) Krichels, A. H.; Yang, W. H. Dynamic controls on field-scale soil nitrous oxide hot spots and hot moments across a microtopographic gradient. *J. Geophys. Res.: Biogeosci.* **2019**, *124*, 3618−3634.
(41) Santegoeds, C. M.; Schramm, A.; de Beer, D. d. Microsensors as a tool to determine chemical microgradients and bacterial activity in wastewater biofilms and flocs. *Biodegradation* **1998**, *9*, 159−167.
(42) Li, T.; Piltz, B.; Podola, B.; Dron, A.; de Beer, D.; Melkonian, M. Microscale profiling of photosynthesis-related variables in a highly productive biofilm photobioreactor. *Biotechnol. Bioeng.* **2016**, *113*, 1046−1055.
(43) Johnson, S. L.; Neuer, S.; Garcia-Pichel, F. Export of nitrogenous compounds due to incomplete cycling within biological soil crusts of arid lands. *Environ. Microbiol.* **2007**, *9*, 680−689.
(44) Rundel, P. W.; Cowling, R. M., Biodiversity of the Succulent Karoo. In *Encyclopedia of Biodiversity* 2nd Ed, Levin, S. A., Ed. Academic Press: Waltham, 2013; pp 485-490.
(45) Haarmeyer, D. H.; Schmiedel, U.; Dengler, J.; Bösing, B. M. How does grazing intensity affect different vegetation types in arid Succulent Karoo, South Africa? Implications for conservation management. *Biol. Conserv.* **2010**, *143*, 588−596.
(46) Jürgens, N.; Haarmeyer, D. H.; Luther-Mosebach, J.; Dengler, J.; Finckh, M.; Schmiedel, U., Biodiversity in southern Africa. *Patterns at local scale - the BIOTA Observatories*; Klaus Hess Publishers: 2010, Vol. *1*, p 801.
(47) Henschel, J. R.; Hoffman, M. T.; Walker, C. Introduction to the Karoo Special Issue: Trajectories of change in the Anthropocene. *Afr. J. Range Forage Sci.* **2018**, *35*, 151−156.
(48) Myers, N.; Mittermeier, R. A.; Mittermeier, C. G.; da Fonseca, G. A. B.; Kent, J. Biodiversity hotspots for conservation priorities. *Nature* **2000**, *403*, 853−858.
(49) Rodríguez-Caballero, E.; Reyes, A.; Kratz, A. M.; Caesar, J.; Guirado, E.; Schmiedel, U.; Escribano, P.; Fiedler, S.; Weber, B. Effects of climate change and land use intensification on regional biological soil crust cover and composition in southern Africa. *Geoderma* **2022**, *406*, 115508.
(50) de Beer, D., Potentiometric microsensors for in situ measurements in aquatic environments. In *In Situ Monitoring of Aquatic Systems : Chemical Analysis and Speciation*, Buffle, J.; Horvai, G., Eds. Wiley & Sons: London, 2000; pp 161-194.
(51) De Beer, D.; Schramm, A.; Santegoeds, C. M.; Kuhl, M. A nitrite microsensor for profiling environmental biofilms. *Appl. Environ. Microbiol.* **1997**, *63*, 973−977.
(52) de Beer, D.; van den Heuvel, J. C. Response of ammonium-selective microelectrodes based on the neutral carrier nonactin. *Talanta* **1988**, *35*, 728−730.
(53) Johansson, O.; Olofsson, J.; Giesler, R.; Palmqvist, K. Lichen responses to nitrogen and phosphorus additions can be explained by the different symbiont responses. *New Phytol.* **2011**, *191*, 795−805.
(54) Tamm, C. O. *Growth, yield and nutrition in carpets of a forest moss (Hylocomium splendens)*, 1953, Meddelanden från Statens skogsforskningsinstitut, *43* (1), 1-140.
(55) Rodríguez-Caballero, E.; Aguilar, M. Á.; Castilla, Y. C.; Chamizo, S.; Aguilar, F. J. Swelling of biocrusts upon wetting induces changes in surface micro-topography. *Soil Biol. Biochem.* **2015**, *82*, 107−111.
(56) Menon, M.; Yuan, Q.; Jia, X.; Dougill, A. J.; Hoon, S. R.; Thomas, A. D.; Williams, R. A. Assessment of physical and hydrological properties of biological soil crusts using X-ray microtomography and modeling. *J. Hydrol.* **2011**, *397*, 47−54.
(57) Coppola, A.; Basile, A.; Wang, X.; Comegna, V.; Tedeschi, A.; Mele, G.; Comegna, A. Hydrological behaviour of microbiotic crusts on sand dunes: Example from NW China comparing infiltration in crusted and crust-removed soil. *Soil Tillage Res.* **2011**, *117*, 34−43.
(58) Felde, V. J. M. N. L.; Peth, S.; Uteau-Puschmann, D.; Drahorad, S.; Felix-Henningsen, P. Soil microstructure as an under-explored feature of biological soil crust hydrological properties: case study from the NW Negev Desert. *Biodivers. Conserv.* **2014**, *23*, 1687−1708.
(59) Couradeau, E.; Felde, V.; Parkinson, D.; Uteau, D.; Rochet, A.; Cuellar, C.; Winegar, G.; Peth, S.; Northen, T.; Garcia-Pichel, F. In situ X-ray tomography imaging of soil water and cyanobacteria from biological soil crusts undergoing desiccation. *Front. Environ. Sci.* **2018**, *6* (65), DOI: 10.3389/fenvs.2018.0006.
(60) Deng, J.; Orner, E. P.; Chau, J. F.; Anderson, E. M.; Kadilak, A. L.; Rubinstein, R. L.; Bouchillon, G. M.; Goodwin, R. A.; Gage, D. J.; Shor, L. M. Synergistic effects of soil microstructure and bacterial EPS on drying rate in emulated soil micromodels. *Soil Biol. Biochem.* **2015**, *83*, 116−124.

(61) Garcia-Pichel, F.; Sherry, N. D.; Castenholz, R. W. Evidence for an ultraviolet sunscreen role of the extracellular pigment scytonemin in the terrestrial cyanobacterium *Chlorogloeopsis* sp. *Photochem. Photobiol.* **1992**, *56*, 17−23.
(62) Garcia-Pichel, F.; Castenholz, R. W. Characterization and biological implications of scytonemin, a cyanobacterial sheath pigment. *J. Phycol.* **1991**, *27*, 395−409.
(63) Flemming, H.-C.; Wingender, J. The biofilm matrix. *Nat. Rev. Microbiol.* **2010**, *8*, 623−633.
(64) Roberson, E. B.; Firestone, M. K. Relationship between desiccation and exopolysaccharide production in a soil *Pseudomonas* sp. *Appl. Environ. Microbiol.* **1992**, *58*, 1284−1291.
(65) Pereira, S.; Zille, A.; Micheletti, E.; Moradas-Ferreira, P.; De Philippis, R.; Tamagnini, P. Complexity of cyanobacterial exopolysaccharides: composition, structures, inducing factors and putative genes involved in their biosynthesis and assembly. *FEMS Microbiol. Rev.* **2009**, *33*, 917−941.
(66) Rossi, F.; Mugnai, G.; De Philippis, R. Complex role of the polymeric matrix in biological soil crusts. *Plant Soil* **2018**, *429*, 19−34.
(67) Adessi, A.; Cruz de Carvalho, R.; De Philippis, R.; Branquinho, C.; Marques da Silva, J. Microbial extracellular polymeric substances improve water retention in dryland biological soil crusts. *Soil Biol. Biochem.* **2018**, *116*, 67−69.
(68) D'Odorico, P.; Laio, F.; Porporato, A.; Rodriguez-Iturbe, I. Hydrologic controls on soil carbon and nitrogen cycles. II. A case study. *Adv. Water Resour.* **2003**, *26*, 59−70.
(69) Couradeau, E.; Giraldo-Silva, A.; De Martini, F.; Garcia-Pichel, F. Spatial segregation of the biological soil crust microbiome around its foundational cyanobacterium, *Microcoleus vaginatus*, and the formation of a nitrogen-fixing cyanosphere. *Microbiome* **2019**, *7*, 55.
(70) Garcia-Pichel, F.; Johnson, S. L.; Youngkin, D.; Belnap, J. Small-scale vertical distribution of bacterial biomass and diversity in biological soil crusts from arid lands in the Colorado Plateau. *Microb. Ecol.* **2003**, *46*, 312−321.
(71) Garcia-Pichel, F.; Belnap, J. Microenvironments and microscale productivity of cyanobacterial desert crusts. *J. Phycol.* **1996**, *32*, 774−782.
(72) Garcia-Pichel, F.; Belnap, J., Small-scale environments and distribution of biological soil crusts. In *Biological soil crusts: Structure, function, and management*, Belnap, J.; Lange, O. L., Eds. Springer Berlin Heidelberg: Berlin, Heidelberg, 2003; pp 193-201.
(73) Nunan, N.; Young, I. M.; Crawford, J. W.; Ritz, K., Bacterial interactions at the microscale - linking habitat to function in soil. In *The spatial distribution of microbes in the environment*, Franklin, R. B.; Mills, A. L., Eds. Springer: Dordrecht, 2007; pp 61-85.
(74) Nunan, N.; Wu, K.; Young, I. M.; Crawford, J. W.; Ritz, K. Spatial distribution of bacterial communities and their relationships with the micro-architecture of soil. *FEMS Microbiol. Ecol.* **2003**, *44*, 203−215.
(75) Sessitsch, A.; Weilharter, A.; Gerzabek, M. H.; Kirchmann, H.; Kandeler, E. Microbial population structures in soil particle size fractions of a long-term fertilizer field experiment. *Appl. Environ. Microbiol.* **2001**, *67*, 4215−4224.
(76) Or, D.; Smets, B. F.; Wraith, J. M.; Dechesne, A.; Friedman, S. P. Physical constraints affecting bacterial habitats and activity in unsaturated porous media − a review. *Adv. Water Resour.* **2007**, *30*, 1505−1527.
(77) Tecon, R.; Or, D. Biophysical processes supporting the diversity of microbial life in soil. *FEMS Microbiol. Rev.* **2017**, *41*, 599−623.
(78) Grundmann, G. L.; Debouzie, D. Geostatistical analysis of the distribution of NH_4^+ and NO_2^--oxidizing bacteria and serotypes at the millimeter scale along a soil transect. *FEMS Microbiol. Ecol.* **2000**, *34*, 57−62.
(79) Ranjard, L.; Richaume, A. Quantitative and qualitative microscale distribution of bacteria in soil. *Microbiol. Res.* **2001**, *152*, 707−716.
(80) Chenu, C.; Stotzky, G., Interactions between microorganisms and soil particles: an overview. In *Interactions between soil particles and microorganisms: Impact on the terrestrial ecosystem*, Huang, P. M.; Bollag, J.-M.; Senesi, N., Eds. John Wiley & Sons Ltd: Chichester, U.K., 2001; pp 3-40.
(81) Mummey, D.; Holben, W.; Six, J.; Stahl, P. Spatial stratification of soil bacterial populations in aggregates of diverse soils. *Microb. Ecol.* **2006**, *51*, 404−411.
(82) Kanazawa, S.; Filip, Z. Distribution of microorganisms, total biomass, and enzyme activities in different particles of brown soil. *Microb. Ecol.* **1986**, *12*, 205−215.
(83) Ruamps, L. S.; Nunan, N.; Chenu, C. Microbial biogeography at the soil pore scale. *Soil Biol. Biochem.* **2011**, *43*, 280−286.
(84) Raynaud, X.; Nunan, N. Spatial Ecology of Bacteria at the Microscale in Soil. *PLOS ONE* **2014**, *9*, No. e87217.
(85) Chenu, C.; Hassink, J.; Bloem, J. Short-term changes in the spatial distribution of microorganisms in soil aggregates as affected by glucose addition. *Biol. Fertil. Soils* **2001**, *34*, 349−356.
(86) Grundmann, H.; Hori, S.; Tanner, G. Determining confidence intervals when measuring genetic diversity and the discriminatory abilities of typing methods for microorganisms. *J. Clin. Microbiol.* **2001**, *39*, 4190.
(87) Bowker, M. A.; Belnap, J.; Büdel, B.; Sannier, C.; Pietrasiak, N.; Eldridge, D. J.; Rivera-Aguilar, V., Controls on distribution patterns of biological soil crusts at micro- to global scales. In *Biological soil crusts: An organizing principle in drylands*, Weber, B.; Büdel, B.; Belnap, J., Eds. Springer International Publishing: Cham, 2016; pp 173-197.
(88) Garcia-Pichel, F.; Felde, V. J. M. N. L.; Drahorad, S. L.; Weber, B., Microstructure and weathering processes within biological soil crusts. In *Biological Soil Crusts: An Organizing Principle in Drylands*, Weber, B.; Büdel, B.; Belnap, J., Eds. Springer International Publishing: Cham, 2016; pp 237-255.
(89) Tiedje, J. M.; Sexstone, A. J.; Parkin, T. B.; Revsbech, N. P.; Shelton, D. R. Anaerobic processes in soil. *Plant Soil* **1984**, *76*, 197−212.
(90) Abed, R. M. M.; Polerecky, L.; Al-Habsi, A.; Oetjen, J.; Strous, M.; de Beer, D. Rapid recovery of cyanobacterial pigments in desiccated biological soil crusts following addition of water. *PLOS ONE* **2014**, *9*, No. e112372.
(91) Scherer, S.; Ernst, A.; Chen, T.-W.; Böger, P. Rewetting of drought-resistant blue-green algae: Time course of water uptake and reappearance of respiration, photosynthesis, and nitrogen fixation. *Oecologia* **1984**, *62*, 418−423.
(92) Angel, R.; Matthies, D.; Conrad, R. Activation of methanogenesis in arid biological soil crusts despite the presence of oxygen. *PLOS ONE* **2011**, *6*, No. e20453.
(93) Placella, S. A.; Brodie, E. L.; Firestone, M. K. Rainfall-induced carbon dioxide pulses result from sequential resuscitation of phylogenetically clustered microbial groups. *Proc. Natl. Acad. Sci. U. S. A.* **2012**, *109*, 10931−10936.
(94) Cruz-Martínez, K.; Rosling, A.; Zhang, Y.; Song, M.; Andersen, G. L.; Banfield, J. F. Effect of Rainfall-Induced Soil Geochemistry Dynamics on Grassland Soil Microbial Communities. *Appl. Environ. Microbiol.* **2012**, *78*, 7587.
(95) Šťovíček, A.; Kim, M.; Or, D.; Gillor, O. Microbial community response to hydration-desiccation cycles in desert soil. *Sci. Rep.* **2017**, *7*, 45735.
(96) Barnard, R. L.; Osborne, C. A.; Firestone, M. K. Responses of soil bacterial and fungal communities to extreme desiccation and rewetting. *ISME J.* **2013**, *7*, 2229−2241.
(97) McClain, M. E.; Boyer, E. W.; Dent, C. L.; Gergel, S. E.; Grimm, N. B.; Groffman, P. M.; Hart, S. C.; Harvey, J. W.; Johnston, C. A.; Mayorga, E.; McDowell, W. H.; Pinay, G. Biogeochemical Hot Spots and Hot Moments at the Interface of Terrestrial and Aquatic Ecosystems. *Ecosystems* **2003**, *6*, 301−312.
(98) Ebrahimi, A.; Or, D. Microbial community dynamics in soil aggregates shape biogeochemical gas fluxes from soil profiles − upscaling an aggregate biophysical model. *GCB* **2016**, *22*, 3141−3156.
(99) Ebrahimi, A.; Or, D. Dynamics of soil biogeochemical gas emissions shaped by remolded aggregate sizes and carbon configurations under hydration cycles. *GCB* **2018**, *24*, e378−e392.

(100) Kim, M.; Or, D. Microscale pH variations during drying of soils and desert biocrusts affect HONO and NH_3 emissions. *Nat. Commun.* **2019**, *10*, 3944.
(101) Kim, M.; Or, D. Hydration status and diurnal trophic interactions shape microbial community function in desert biocrusts. *Biogeosciences* **2017**, *14*, 5403−5424.
(102) Shammas, N. K. Interactions of temperature, pH, and biomass on the nitrification process. *J Water Pollut Control Fed* **1986**, *58*, 52−59.
(103) Parkin, T. B. Soil microsites as a source of denitrification variability. *Soil Sci. Soc. Am. J.* **1987**, *51*, 1194−1199.
(104) Højberg, O.; Revsbech, N. P.; Tiedje, J. M. Denitrification in Soil Aggregates Analyzed with Microsensors for Nitrous Oxide and Oxygen. *Soil Sci. Soc. Am. J.* **1994**, *58*, 1691−1698.

https://doi.org/10.1021/acs.est.2c02207
Environ. Sci. Technol. 2022, 56, 11865−11877